

Changes in the Deep Western Boundary Current at 53°N

PAUL G. MYERS

Department of Earth and Atmospheric Sciences, University of Alberta, Edmonton, Alberta, Canada

NILGUN KULAN

ASL Environmental Sciences, Victoria, British Columbia, Canada

(Manuscript received 10 May 2011, in final form 13 March 2012)

ABSTRACT

Southward transports in the deep western boundary current across 53°N, over 1949–99, are determined from a historical reconstruction. Long-term mean transports, for given water masses, for net southward transport (the southward component of the transport not including recirculation given in parentheses) are 4.7 ± 2.3 Sv (5.1 ± 2.4 Sv) ($\text{Sv} \equiv 10^6 \text{ m}^3 \text{ s}^{-1}$) for the Denmark Strait Overflow Water, 6.1 ± 2.7 Sv (6.8 ± 1.7 Sv) for the Iceland–Scotland Overflow Water, 6.5 ± 2.6 Sv (7.1 ± 1.8 Sv) for classical Labrador Sea Water, and 2.3 ± 1.9 Sv (2.7 ± 3.4 Sv) for upper Labrador Sea Water. The estimates take into account seasonal and interannual variability of the isopycnal positions and suggest the importance of including this factor. A strong correlation, 0.91, is found between variability of the total and baroclinic transports (with the barotropic velocity removed) at the annual time scale. This correlation drops to 0.32 if the baroclinic transports are, instead, computed based upon the use of a fixed level of no motion at 1400 m. The Labrador Sea Water layer shows significant variability and enhanced transport during the 1990s but no trend. The deeper layers do show a declining (but nonstatistically significant) trend over the period analyzed, largest in the ISOW layer. The Iceland–Scotland Overflow Water presents a 0.029 Sv yr^{-1} decline or 1.5 Sv over the 50-yr period, an 18%–22% decrease in its mean transport.

1. Introduction

The deep western boundary current (DWBC) transports waters formed by wintertime convection in the northern reaches of the Atlantic Ocean southward toward the equator (Dengler et al. 2006). This transport forms the lower limb of the Atlantic meridional overturning circulation (AMOC) and is balanced by the transport of warm water northward above the thermocline (e.g., Hirschi and Marotzke 2007). A weakening of this circulation, such as by increased freshwater provision to the North Atlantic Ocean, may impact heat transport and climate in eastern North America and Europe (Wu et al. 2007).

The AMOC is a measure of the total northward/southward flow in the Atlantic Ocean, integrated over depth and latitude (Hirschi and Marotzke 2007). Its

importance includes its ability to transport heat to higher latitudes, as well as take up atmospheric gases such as CO_2 and transport them to the deep ocean (Broecker 1997). Many modeling studies suggest it is vulnerable to the input of freshwater at high latitudes where the deep waters are ventilated (e.g. Rooth 1982; Spence et al. 2008; Wu et al. 2007). With changes at high latitude due to climate warming, coupled climate models based on Intergovernmental Panel on Climate Change scenarios suggest that such a weakening is likely to occur in the near future (Solomon et al. 2007).

Evidence for whether such a weakening is presently occurring is hard to come by. Bryden et al. (2005) analyzed five transatlantic sections at 25°N and suggested a reduction in strength of the AMOC by close to 30% between 1957 and 2004. However, based upon a year worth of measurement from the Rapid Climate Change (RAPID) array, Kanzow et al. (2010) showed tremendous intra-annual variability in the overturning at 26.5°N, suggesting that differences between repeat synoptic sections may measure short-term variability rather than a long-term trend. Further studies have focused

Corresponding author address: Paul G. Myers, Department Earth and Atmospheric Sciences, University of Alberta, Edmonton AB, Canada.
E-mail: pmyers@ualberta.ca

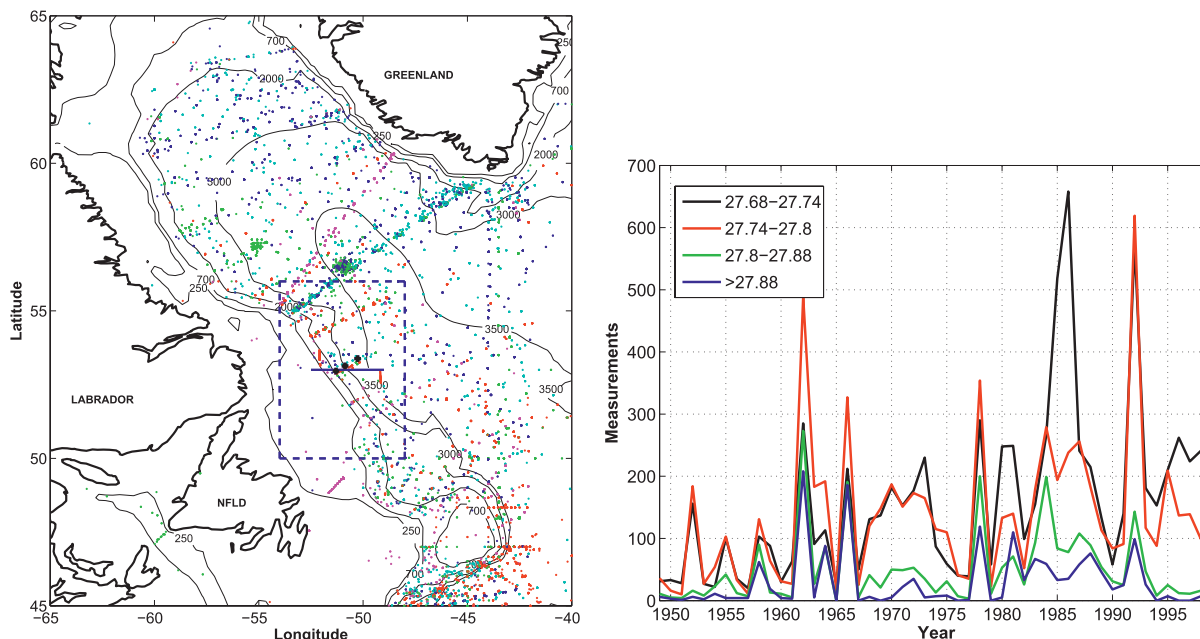
BAFFIN
ISLAND

FIG. 1. (a) Map of the Labrador Sea showing the location of the section used to estimate transports at 53°N (solid line). The dots indicate locations of observations within the deepest layers ($\sigma_{\theta} > 27.8 \text{ kg m}^{-3}$) used in the objective analysis, with the color indicating the decade when the observation was made: 1950s (cyan), 1960s (blue), 1970s (green), 1980s (red), and 1990s (maroon). The plus symbols indicate the location of the 53°N mooring line (Dengler et al. 2006) and the dashed box indicates the area used to count the number of measurements in the objective analysis, shown in the right panel for each density layer and year.

only on the deep western boundary current, the part of the meridional circulation flowing southward in a strong, narrow current along the base of the continental slope of Greenland/North America. Examining the deepest components of the DWBC south of Greenland, associated with the Nordic Seas overflows, Bacon (1998) identified significant decadal variability, associated with changes in polar air temperature, but no trend. Kieke and Rhein (2006) found significant interannual variability in the baroclinic transport associated with an increase from the 1950s to the 1980s, but then a decline in the 1990s. Sarafanov et al. (2009) confirmed the decadal variability and, in fact, observed an enhancement of the deep transport in the 2000s. Within the Labrador Sea Kieke and Rhein (2006) found that the baroclinic component of the DWBC had stronger temporal variability than in the Irminger Sea but were unsure how to interpret the results because of a lack of knowledge of the variability of the velocity at their reference level. In the shallower layers associated with Labrador Sea Water (LSW), although a long-term freshening has been observed (Dickson et al. 2002), significant variability is also present, including during the late 1980s/early 1990s when the most voluminous

and dense class of LSW was formed (Yashayaev et al. 2007).

Fischer et al. (2004) attempted to quantify the circulation at the southern exit of the Labrador Sea at 53°N using ship measurements and a moored current meter array (Fig. 1, left). They (Fischer et al.) showed that there was a well-defined deep western boundary current, including an intense deep core associated with the Denmark Strait Overflow Water (DSOW). This analysis also gave the total deep-water transport from 1997 to 1999 as $26 \pm 5 \text{ Sv}$ ($\text{Sv} \equiv 10^6 \text{ m}^3 \text{ s}^{-1}$) with an offshore northward recirculation of 9 Sv. Dengler et al. (2006) extended the analysis at 53°N to consider interannual variability and showed a systematic increase (of 15%) in the transport strength post 1999 compared to the prior period. Using over a decade of data for the same section, Fischer et al. (2010) showed the existence of intra-annual to interannual variability but no lower frequency variability or trends. Meanwhile, Han et al. (2010) combined hydrographic data with satellite altimetry to the north of 53°N at Hamilton Bank to show a significant transport decline in the 1990s followed by a smaller rebound in the early 2000s [except in the Iceland–Scotland Overflow Water (ISOW) layer].

To attempt to extend the record and put the recent observations of changes in the deep Labrador Current at 53°N into a historical perspective, we examine this section using a detailed high-resolution historical reconstruction of the Labrador Sea.

2. Historical reconstruction

We use the high-resolution regional climatology of Kulan and Myers (2009) as the basis for our analysis. This product is based on all available temperature and salinity data available in the Marine Environmental Data Service (MEDS) database (Gregory 2004) prior to April 2002 (the date when the production of this climatology was commenced). All data used is thus quality controlled, although there may still be questions about the quality of the data from earlier periods. Additional quality control, including dealing with biases from Ocean Weather Station Bravo (and some other frequently visited stations and sections), was carried out as discussed in Kulan and Myers (2009). Data were then binned into 2.5° (south of 55°N) or 5.0° boxes (north of 55°N) to provide a first guess for an objective analysis procedure, using 44 isopycnal layers in the vertical and $\frac{1}{3}^\circ$ spatial resolution. The vertical resolution includes 14 layers between $\sigma_\theta = 27.4$ and 27.8 kg m^{-3} , with a resolution of 0.05 kg m^{-3} , increased to 0.03 kg m^{-3} for $\sigma_\theta = 27.7\text{--}27.95$ to better resolve the LSW and the deep overflow layers. Given the limitations of available data (discussed in more detail below), a higher vertical resolution would not have been practical. The first guess fields were then corrected progressively for each isopycnal layer with three passes using decreasing correlation lengths of 500, 300, and 150 km, weighted by a severe topographic constraint to minimize mixing of waters across the shelf break.

An additional mapping was carried out for overlapping 3-yr running mean periods (triads) between 1949 and 1999. As described in Myers and Donnelly (2008), each triad was defined to include all data collected in a given year, as well as all available data in the preceding and following year. The mapping procedure was repeated, using the long-term climatology as the first guess field, as described above (and in Kulan and Myers 2009) for each triad, except with larger correlation lengths (of 600, 400, and 200 km), to account for the reduced amounts of data available for shorter time periods.

These fields were then assimilated into a regional model (with $\frac{1}{3}^\circ$ horizontal resolution and 36 unequally spaced levels in the vertical) of the subpolar gyre (Myers 2002) using spectral nudging (Thompson et al. 2006).

Details of the underlying model and forcing, as well as a validation, are given in Myers et al. (2009). Taking advantage of the properties of spectral nudging, we only nudge the mean annual cycle (with a nudging time scale of 10 days). Additionally the nudges are spatially filtered using seven passes of a fourth-order Butterworth filter so that the smallest scales (and thus resolved component of the mesoscale variability) were not impacted. To deal with any possible transient spinup effects as the nudging was turned on, the model is integrated for five repeated years for each year of the reconstruction, starting from the fields from the end of the previous year. The first year (1949) is initialized from a model run nudged to the mean climatological fields using perpetual year forcing.

Although the data is biased toward the upper layers, if we examine the data density in a box around the 53°N section (Fig. 1, left), we see that there is data for every water mass every year except for the densest layer, which is missing data in nine years (Fig. 1, right). Looking at the spatial distribution shows various observational lines across the boundary currents and the interior of the Labrador Sea. Although this figure combines the two deepest layers, it shows that in all decades there is some data for the deepest layers within the region around 53°N or upstream of it (thus allowing the information from the data to propagate to 53°N). We would thus expect the historical reconstruction to be constrained to flow fields consistent with the observations (as was shown in previous studies; e.g., Myers et al. 2009).

Kulan and Myers (2009) showed the mean temperature and salinity from their reconstruction projected onto the World Ocean Circulation Experiment AR7W line was consistent with observational sections. To further look at adequacy of the deeper layers in the historical reconstruction, we follow Yashayaev and Loder (2009) and plot temperature salinity over depth as a function of time, averaged over the interior of the Labrador Sea in water depths greater than 3000 m (Fig. 2). We see the same general structures as Yashayaev and Loder, with high temperatures and salinities throughout most of the water column around 1970, followed in the upper and intermediate layers with fresh (and cold) periods between 1973 and 1982 and post 1986. In the deepest layers, we see a general decline of salinity from 1970 to the end of the record in 1999, as well as a slow increase in temperature over the same period. Although this is a qualitative comparison, the broad consistency between the historical reconstruction and the data analysis suggests that the model is able to maintain the general properties of the observed fields and the long-term low frequency variability, even in the deeper layers.

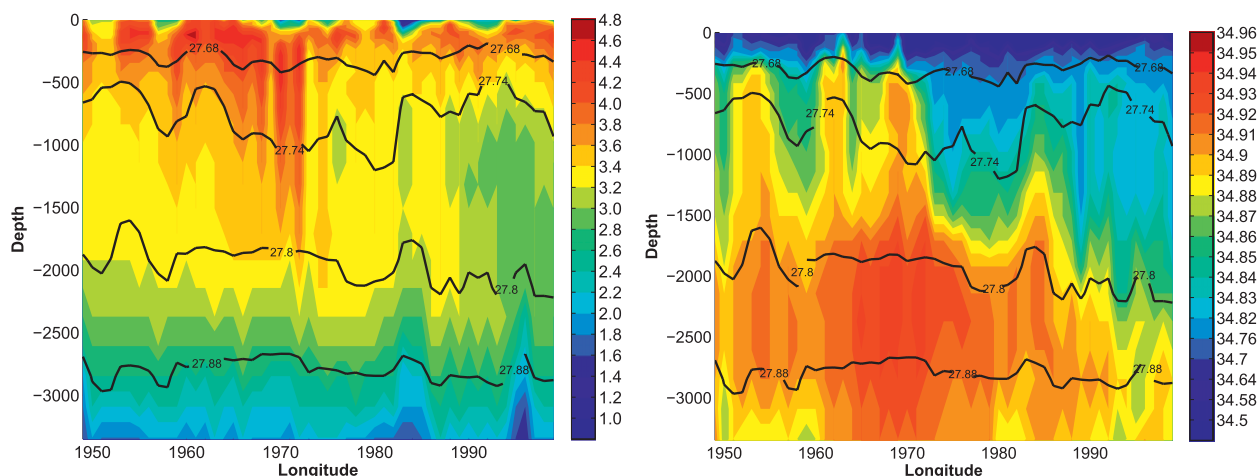


FIG. 2. Time vs depth plots of (a) temperature and (b) salinity from the last month of integration for each year of the historical reconstruction, averaged over the interior (depth > 3000 m) of the Labrador Sea. The solid black lines are the bounding isopycnals for the main water masses discussed in the text.

We follow the approach of Dengler et al. (2006) to estimate errors. Velocity standard deviations are estimated for each model grid point each year (based on 73 five-day output snapshots). Uncertainties are then estimated using a Monte Carlo method with 100 draws. For each five-day snapshot over the entire 1949–99 period, we use a random velocity uncertainty by assuming a Gaussian distribution scaled to the velocity standard deviation for that grid cell and year. The standard deviations of the resulting layer transports over all draws are then calculated and used as a measure of the transport uncertainty. The velocity standard deviations are shown in Fig. 3 and are in the range of $0.02\text{--}0.04\text{ m s}^{-1}$. These variations are smaller than the $0.05\text{--}0.08\text{ m s}^{-1}$ found by Dengler et al. (2006) and are probably associated with the features resolved in the model rather than a true uncertainty in the model's reproduction of the actual variability.

3. Labrador Current at 53°N

Current velocity and volume transports calculated from the historical reconstruction along a section at 53°N , averaged from 1996 to 1999 (to allow a direct comparison with Dengler et al. 2006), are given in Fig. 3. The layers that we focus on are the Denmark Strait Overflow Water (DSOW) ($\sigma_\theta > 27.88$), Iceland–Scotland Overflow Water (ISOW) ($27.8 < \sigma_\theta < 27.88$), as well as classical Labrador Sea Water (cLSW) ($27.74 < \sigma_\theta < 27.8$), and upper Labrador Sea Water (uLSW) ($27.68 < \sigma_\theta < 27.74$).

The strongest net southward transports (the southward component of the transport not including recirculation

given in parentheses) during this 4-yr period are in the LSW layers, with $10.6 \pm 2.3\text{ Sv}$ ($11.9 \pm 1.8\text{ Sv}$) of cLSW transported southward, in addition to $3.2 \pm 1.4\text{ Sv}$ ($3.5 \pm 3.4\text{ Sv}$) of uLSW. Significant transports are also seen in the deep overflow layers with $5.3 \pm 2.0\text{ Sv}$ ($6.4 \pm 1.7\text{ Sv}$) of ISOW and $4.7 \pm 1.9\text{ Sv}$ ($5.2 \pm 2.4\text{ Sv}$) of DSOW exported southward. We do note that the observational section is inclined (Dengler et al. 2006) while we present results along a zonal section, but we would expect little loss from the DWBC in the short distance between the two sections or significant cross-slope flow. Our combined estimate for southward flow in the two LSW layers is $15.4 \pm 1.8\text{ Sv}$ compared to the 16.2 Sv found by Dengler et al. (2006), while we find $11.6 \pm 2.8\text{ Sv}$ of southward flow for the two deeper overflow layers compared to 11.4 Sv for Dengler et al. If we plot the baroclinic component of the transport in the overflow layers (Fig. 4) during the 1990s, we see a rapid increase in transport within the first 100 km of the slope, with the maximum transport reached 200–250 km off the Labrador Shelf. This pattern, as well as current width, is comparable to that of Kieke and Rhein (2006) (their Fig. 5b). The overall southward dense water transport of $27.6 \pm 4.0\text{ Sv}$ in the boundary current compares well, considering the completely different approaches and gives us confidence that the results of our reconstruction are robust.

However our results for southward transport in the deepest layers are partitioned slightly differently (more in the DSOW layer, 5.2 Sv versus 3.6 Sv , and less in the ISOW layer, 6.4 Sv versus 7.8 Sv). As we wish to consider the temporal variability of the transports in each layer, we need to understand this discrepancy from the

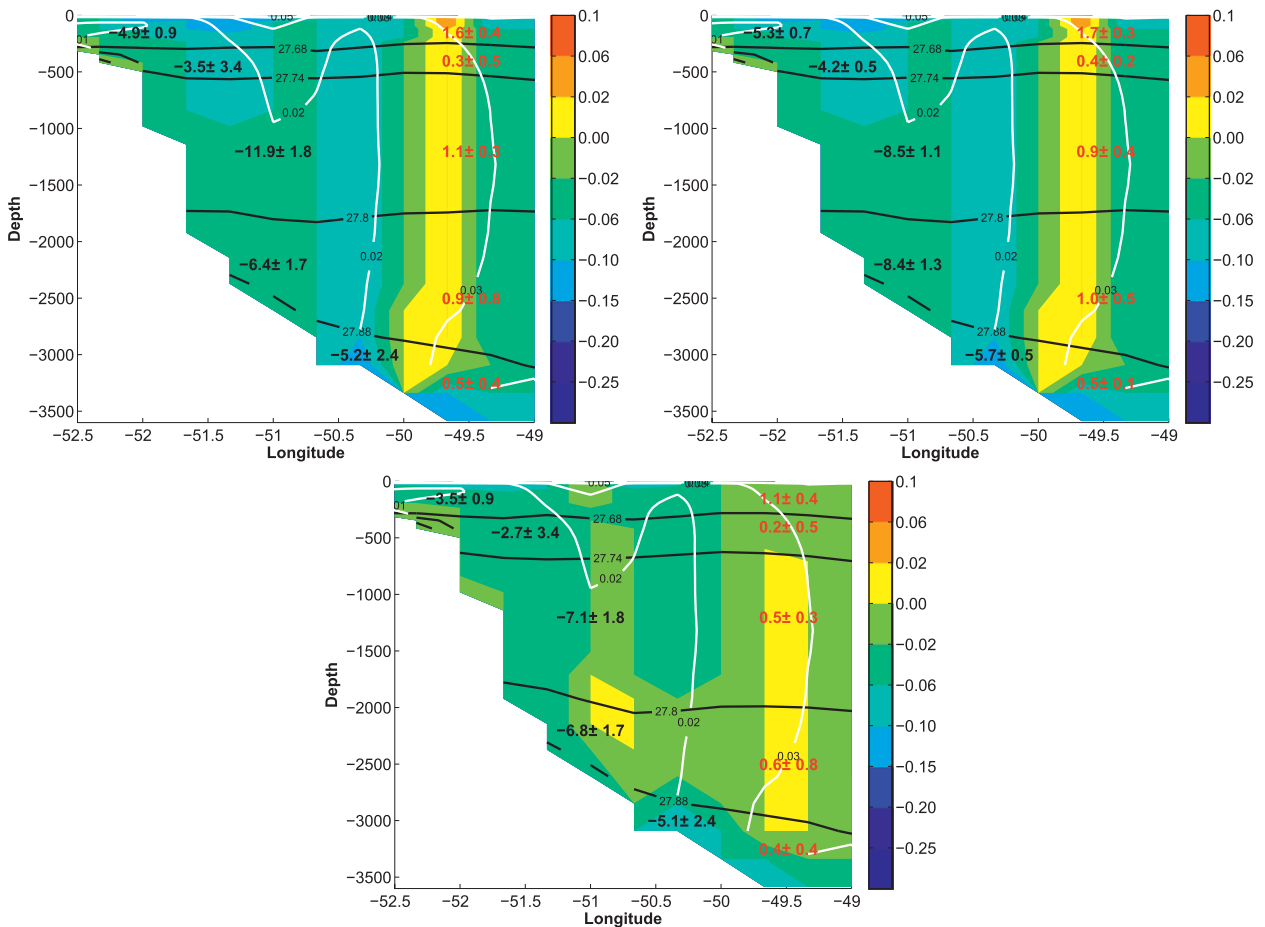


FIG. 3. Longitude vs depth plots at 53°N from the historical reconstruction. The underlying color field is velocity (negative values associated with southward flow) contoured using a variable bin width scale, as shown in the color bar. The white shaded region is the topography. The solid black lines are the bounding isopycnals for the main water masses discussed in the text. The solid white lines are contours of the velocity standard deviation. The large numerical values are the mean transports in each density layer, with uncertainty, for both the western boundary current (black) as well as the countercurrent (red): (top left) the mean over 1996–99, (top right) the mean over 1996–99 but using the climatological isopycnal positions (see text for further details), and (bottom) the mean over the entire analysis period, 1949–99.

observations so as to be sure that any signals that we see are real and not just an artifact of the reconstruction. We first note that the Dengler et al. (2006) estimate is within the uncertainty range from our reconstruction. That said, we think it is important to understand more about the causes of these differences.

One possible cause for the different partitioning may be a function of our estimates taking into account the seasonal and interannual variations in the positions of the isopycnals bounding our layers, something that Dengler et al. (2006) were not able to do. We therefore recalculate our transports over 1996–99 but based on the mean density structure at 53°N from the Kulan and Myers (2009) climatology (i.e., removing all variability in the isopycnal positions), which are given in Fig. 3. There is little change in the DSW transport between

the two approaches, no more than 0.5 Sv which is within the uncertainty of the estimates.

However, there are big changes in the transports in the ISOW and cLSW layers. Our southward cLSW transport has decreased to 8.5 ± 1.1 Sv, while the ISOW estimate has increased to 8.4 ± 1.3 Sv. This new estimate for ISOW is much closer to the 7.8 Sv reported by Dengler et al. (2006) and suggests that our original southward estimate of 6.4 ± 1.7 Sv was not a function of the historical reconstruction underestimating the transport in this layer. Instead, it suggests that the transport estimates are quite sensitive to the structure of the density field used for the partitioning and its variability. Given this, we suggest that, whenever possible, time-varying density fields be used to estimate transport partitioning between different layers/water masses.

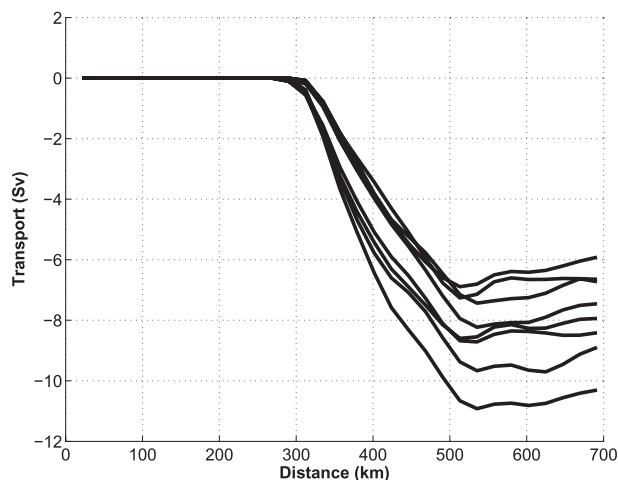


FIG. 4. Plots of the offshelf variations in baroclinic transport, from the historical reconstruction, for eight years in the 1990s. No attempt is made to differentiate between years in the figure, with all years shown for illustrative purpose with respect to the variability.

Long-term means from the historical reconstruction from 1949 to 1999 are presented for the same section in Fig. 3. There are only small changes in the long-term means compared to 1996–99 in the two deepest layers. However the long-term mean net transport of 6.5 ± 2.7 Sv (7.1 ± 1.8 Sv southward) for the cLSW layer is significantly less than for the more recent 1996–99 period. This is to be expected since strong transport at the end of the 1990s is consistent with the dispersal of the voluminous amounts of LSW produced in the early 1990s, given a dispersal time scale of 4–6 yr (Lazier et al. 2002).

The associated transport time series (net and without recirculation) are shown in Figs. 5 and 6. Transport in the cLSW layer varies tremendously, between 3.4 Sv and 14.6 Sv. This variability is consistent with periods of strong LSW formation during the early 1960s as well as the late 1980s/early 1990s. This shows clearly that the high transports of LSW during 1996–99 are a function of the dispersal of the early 1990s class of LSW and are not representative of the entire half century.

Both of the deeper overflow layers show interannual variability, but the amplitude is in general smaller than for the LSW. More interestingly, both of these layers show a fairly steady decline from the 1950s to the end of the 1990s. The decline is most pronounced in the ISOW layer, 0.029 Sv yr⁻¹. The trend in the DSOW layer is smaller at 0.005 yr⁻¹. That said, given the short time records, potential lack of independence of the annual estimates, and large interannual variability, the given trends are not statistically significant. Combining these two layers, we see a reduction in strength of 0.034 Sv yr⁻¹ or a total reduction of 1.7 Sv over the 51-yr period.

This is mainly compensated by an increase of transport in the LSW layer, of 0.03 Sv yr⁻¹, although this may be a function of the strong LSW formation and export in the 1990s—at the end of our study period.

To look at this in more detail, we focus on the baroclinic component of southward transport in the DWBC ($\sigma_\theta > 27.8$) to compare with Kieke and Rhein (2006). First looking at the 1990s (Fig. 7a), we find slightly larger baroclinic transports, reaching 11 Sv in 1996, but smaller interannual variability (4.5 Sv). Like Kieke and Rhein, we see stronger baroclinic transports during 1990–93, with weaker transports post 1996. However, the interannual fluctuations do not seem in phase and, potentially more troubling, we find the largest baroclinic transports in 1995 and 1996, years of low transport in the Kieke and Rhein (2006) analysis. Looking at the 1950s and 1960s, we see some features reported by Kieke and Rhein, such as weaker baroclinic transports in 1951–52 (but still much larger than the Kieke and Rhein < 3 Sv, strong baroclinic transports in 1953–54, and weak baroclinic transports in 1957–58. We see little of the variability reported by Kieke and Rhein (2006) in the 1960s, including their finding of > 11 Sv in 1964.

Before we decide that these discrepancies imply that our historical reconstruction is weak, we consider that Kieke and Rhein computed their baroclinic transports based on the assumption of a time-invariant level of no motion at 1400 m (which they knew was unrealistic but, having no velocity data, were forced to use). Our baroclinic transports reported above are instead based on just removing the model barotropic component from the total absolute velocities. To compare, we recompute our baroclinic transports using the baroclinic geostrophic velocities obtained from the 5-day outputs of model density from the historical analysis and using a level of no motion at 1400 m (Fig. 7, right). We now see a range of transports between 2.5 Sv and 13 Sv, comparable to Kieke and Rhein (2006). To examine the phasing, we focus on the 3-yr running mean curve since our density fields are based on averaging over 3-yr running mean triads. For the 1990s our southward baroclinic transports, relative to 1400 m, peak in 1992 at 9 Sv before decreasing to under 6 Sv in 1996–97, consistent with Kieke and Rhein, although we still do not see their extreme minimum in 1995 (noting that there is no deep data included in the triad analysis for this year). Additionally, general features of the Kieke and Rhein early estimates, such as stronger baroclinic transports in the early 1950s and weaker transports in the late 1950s, are now seen. Our peak in the 1960s still does not correspond to the > 11 Sv seen by Kieke and Rhein (2006) in 1966. We again note that, for some of the years in question, there is very little data in the deeper

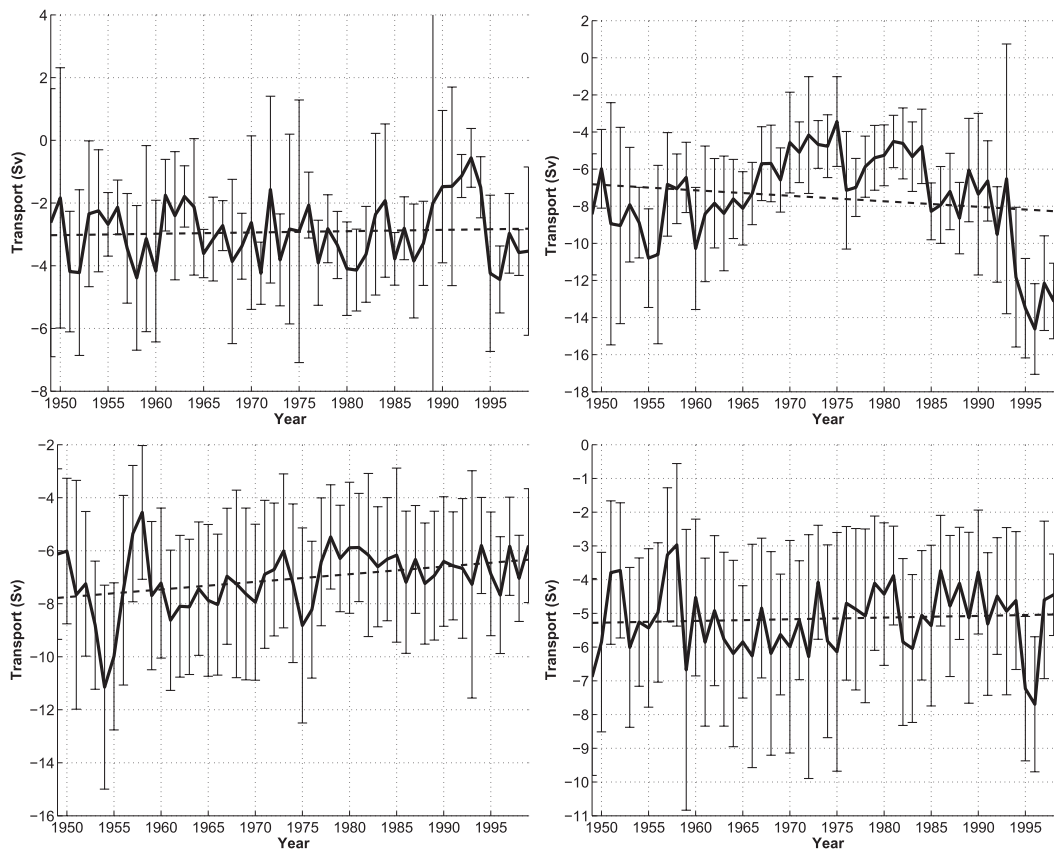


FIG. 5. Time series of southward transports (Sv) at 53°N, for the period 1949–99, from the historical reconstruction, in the (top left) uLSW, (top right) cLSW, (bottom left) ISOW, and (bottom right) DSOw layer. The dashed lines are a linear trend line based on a least squares fit of the data for each layer. Error bars are based on the standard deviations of the layer transport over all draws of the Monte Carlo analysis discussed at the end of section 2.

layers going into the historical reconstruction in the region around 53°N (Fig. 1). This includes parts of the 1950s and 1960s, as well as the later parts of the 1990s [this last being a function of the analysis of Kulan and Myers (2009) being carried out before much of the cruise data became available in the MEDS database].

More generally, we can look at how well the variability in southward transport of the DWBC ($\sigma_\theta > 27.8$) from our analysis agrees between the estimates based on using the total velocities, baroclinic velocities, and baroclinic geostrophic velocities relative to 1400-m estimates. The transports estimates based on the total and baroclinic velocities correlate very well, at the annual time scale, at 0.91, suggesting that much of the overall variability in the deep transport is due to changes in the density structure impacting the baroclinic velocities. The correlation between the transports from the two baroclinic estimates, based upon removing the barotropic velocity from the total velocity and based upon the baroclinic geostrophic velocities relative to 1400 m, is smaller, 0.65. The correlation between the transports

using the baroclinic geostrophic velocities relative to 1400 m and the total velocities is small, 0.32, and barely significant. This suggests that the use of a level of no motion at 1400 m is not justified, with the resulting variability estimates not significantly linked to the actual variability of the DWBC at 53°N. We confirm this by plotting the annually averaged velocities at 53°N from the historical reconstruction (Fig. 8). We see both that the velocity is not zero at this depth and that there is significant interannual variability in the actual velocities.

4. Summary and discussion

Transports in the deep western boundary current across 53°N, over 1996–99 and 1949–99, are determined from a historical reconstruction. Although there are concerns with the use of a reconstruction due to issues with the underlying model and lack of data (especially in the deeper layers), the comparisons presented above suggest that the results here are a step toward improving

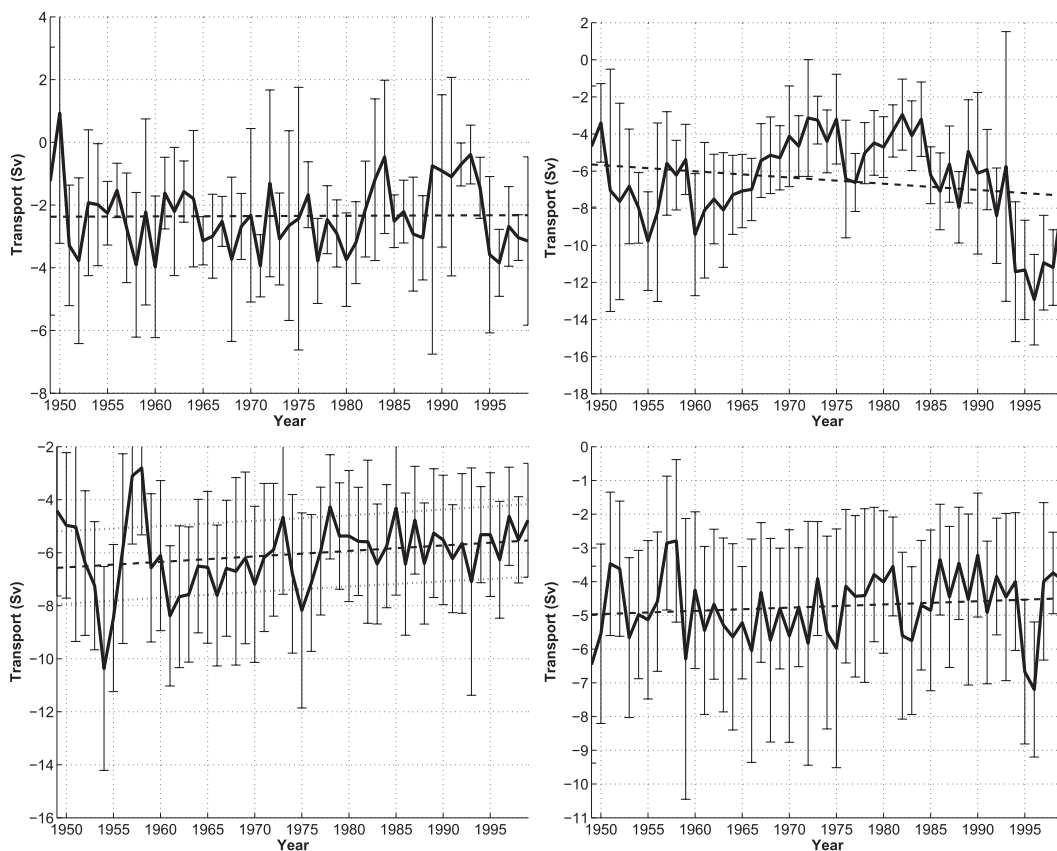


FIG. 6. Time series of net southward transports including recirculation (Sv) for the period 1949–99, from the historical reconstruction at 53°N, in the (top left) uLSW, (top right) cLSW, (bottom left) ISOW, and (bottom right) DSOW layer. The dashed lines are a linear trend line based on a least squares fit of the data for each layer. Error bars are based on the standard deviations of the layer transport over all draws of the Monte Carlo analysis discussed at the end of section 2.

our understanding and knowledge of past variability of the DWBC. Our estimates over 1996–99 agree well with the observational estimates of Dengler et al. (2006). Additionally, we show that the estimates are sensitive to the variability (seasonal and interannual) in the density field used to partition the velocities/transports. Thus, the estimates by Dengler et al. may overestimate the transports in the ISOW layer. Long-term mean transports, over 1996–99, for given water masses, for net southward transport (the southward component of the transport not including recirculation given in parentheses) are 4.7 ± 2.3 Sv (5.1 ± 2.4 Sv) for the Denmark Strait Overflow Water, 6.1 ± 2.7 Sv (6.8 ± 1.7 Sv) for the Iceland–Scotland Overflow Water, 6.5 ± 2.6 Sv (7.1 ± 1.8 Sv) for classical Labrador Sea Water, and 2.3 ± 1.9 Sv (2.7 ± 3.4 Sv) for upper Labrador Sea Water. As the model velocity standard deviation underestimates that from moorings (Dengler et al. 2006), we note that our estimates may underestimate the actual transport uncertainty.

The LSW layers show significant variability and enhanced transport during the 1990s but no trend. The deeper layers show a declining (but not statistically significant) trend over the period analyzed, largest in the ISOW layer, at 0.029 Sv yr⁻¹ or 1.5 Sv over the 50-yr period, an 18%–22% decrease in the mean transport of this layer.

Although Han et al. (2010) found a rebound in the transport at 56°N in the DSOW layer post 2001, they found a near continuous decline in ISOW transport from 1993 to 2004. The rate of decline over the period analyzed by Han et al., 0.067 Sv yr⁻¹, was about double the rate of the long-term decline that we find over 1949–99. Although our use of 3-yr running mean hydrographic data to drive the historical reanalysis may lead to some timing issues for transport variability in individual years, this should not impact the overall long-term changes reported.

We note that our southward transport variability in the DWBC is mainly baroclinic, with a correlation 0.91

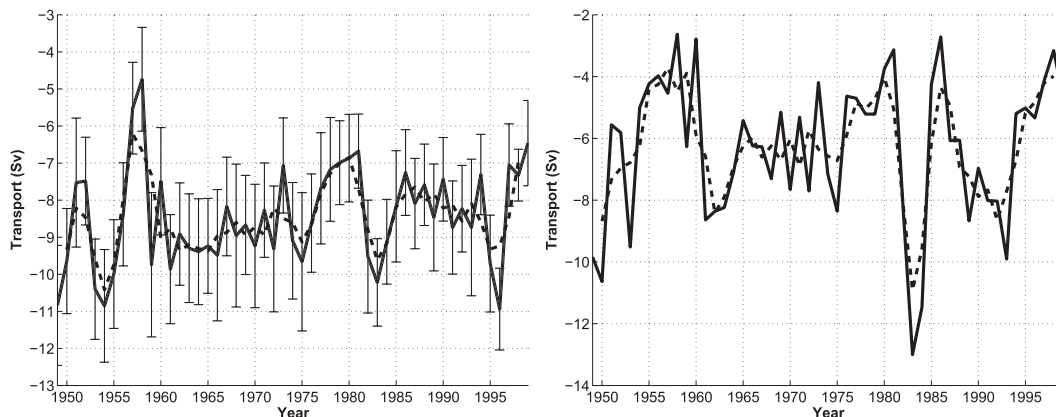


FIG. 7. (left) Time series of baroclinic transports (Sv) for the period 1949–99, from the historical reconstruction at 53°N, for the DWBC (sum of ISOW and DSOW layers), with uncertainty estimates. Error bars are based on the standard deviations of the layer transport over all draws of the Monte Carlo analysis discussed at the end of section 2. The dashed line is the 3-yr running mean. (right) As in the left panel but of baroclinic transports (Sv) based upon baroclinic geostrophic velocities using a reference level of no motion at 1400 m. The dashed line is the 3-yr running mean.

between the transports computed using the total and baroclinic velocities (at the annual time scale). If, instead, we follow the approach commonly used for hydrographic data (due to a lack of direct velocity measurements), of computing the baroclinic geostrophic velocities using a level of no motion, the correlation drops. For example, using the same 1400 m as Kieke and Rhein (2006) (which they admit was an ad hoc choice), the correlation between the resulting transports drops to 0.32. This is because there is no level of no motion at 1400 m in the Labrador Sea. Additionally, there is a significant temporal variability in the velocities at 1400 m that is lost with assuming a time-invariant level of no/known motion. Although difficult in practice, this result suggests that transport estimates for the DWBC in the Labrador Sea (if not elsewhere where a level of no motion is lacking) should be recalculated using a time-varying reference velocity if at all possible.

The deeper layers that show the weakening found here are those associated with the outflow of waters over the sills separating the Nordic Seas from the rest of the North Atlantic. There has been a general warming and decline of convection in the Nordic Seas over the last several decades (Drange et al. 2005). Hansen et al. (2001) find a 20% reduction in the overflow from the Nordic Seas through the Faroe Bank Channel since 1950, which is the source for the ISOW. However, Eldevik et al. (2009) suggest that the variability of the overflows is driven by the Atlantic Water circulating in the Nordic Seas. In any case, the small mean transports of the deep-water overflows, 3.6 Sv for Denmark Strait (Macrandar et al. 2007) and 1.9 Sv for the Iceland–Scotland channels (Osterhus et al. 2001), suggest that the decline seen

in the Labrador Sea may not be related to a change just in the overflows but also in the processes occurring downstream. Since the much larger transports seen in the Labrador Sea come about due to significant entrainment as these waters sink to the deep ocean after overflowing the shallower sills, it is possible that changes in densities and density contrast may affect the strength of the entrainment. Interactions between LSW and ISOW around the Mid-Atlantic Ridge, as discussed by Boessenkool et al. (2007), may impact the long-term transport of ISOW into the Labrador Sea. Transport changes at 53°N could also be related to changes in

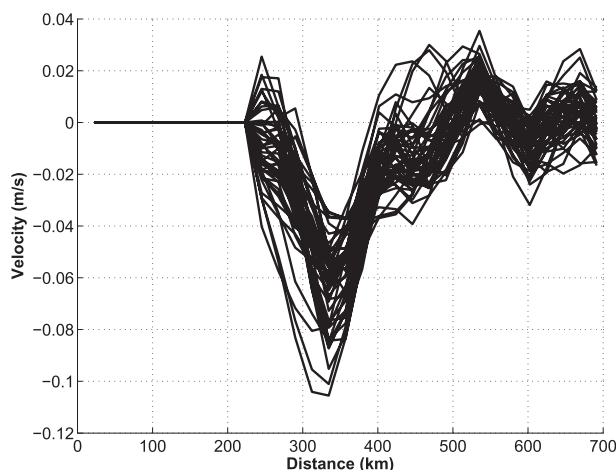


FIG. 8. Line plot of the 1400-m velocities at 53°N. Each line is the annually averaged velocity profile at 53°N from the historical reconstruction. No attempt is made to differentiate between years in the figure, with all years shown for illustrative purpose with respect to the variability.

deep-water circulation in the subpolar gyre, such as changes in the recirculation and path of the deep western boundary current around Cape Farewell and Eirik Ridge (e.g. Holliday et al. 2009).

Acknowledgments. This work was funded by Natural Sciences and Engineering Research Council of Canada (NSERC) and Canadian Foundation for Climate and Atmospheric Sciences (CFCAS) grants (individual as well as through the CLIVAR and GOAPP networks) awarded to PGM. NCEP reanalysis data was provided by the NOAA/OAR/ESRL PSD, Boulder, Colorado, from their website (at <http://www.cdc.noaa.gov/>). We also thank three anonymous reviewers for useful comments that improved this manuscript.

REFERENCES

- Bacon, S., 1998: Decadal variability in the outflow from the Nordic Seas to the deep Atlantic Ocean. *Nature*, **394**, 871–874.
- Boessenkool, K. P., I. R. Hall, H. Elderfield, and I. Yashayaev 2007: North Atlantic climate and deep-ocean flow speed changes during the last 230 years. *Geophys. Res. Lett.*, **34**, L13614, doi:10.1029/2007GL030285.
- Broecker, W. S., 1997: Thermohaline circulation, the Achilles heel of our climate system: Will man-made CO₂ upset the current balance. *Science*, **278**, 1582–1588, doi:10.1126/science.278.5343.1582.
- Bryden, H. L., H. R. Longworth, and S. A. Cunningham, 2005: Slowing of the Atlantic meridional overturning circulation at 25°N. *Nature*, **438**, 655–657, doi:10.1038/nature04385.
- Dengler, M., J. Fischer, F. A. Schott, and R. Zantopp, 2006: Deep Labrador Current and its variability in 1996–2005. *Geophys. Res. Lett.*, **33**, L21S06, doi:10.1029/2006GL026702.
- Dickson, R. R., I. Yashayaev, J. Meincke, B. Turrell, S. Dye, and J. Holfort, 2002: Rapid freshening of the deep North Atlantic Ocean over the past four decades. *Nature*, **416**, 832–837.
- Drange, H., and Coauthors, 2005: The Nordic Seas: An overview. *The Nordic Seas: An Integrated Perspective*, *Geophys. Monogr.*, Vol. 158, Amer. Geophys. Union, 1–10.
- Eldevik, T., J. Nilsen, D. Iovino, K. Olsson, A. Sando, and H. Drange, 2009: Observed sources and variability of Nordic Seas overflow. *Nat. Geosci.*, **2**, 406–410.
- Fischer, J., F. A. Schott, and M. Dengler, 2004: Boundary circulation at the exit of the Labrador Sea. *J. Phys. Oceanogr.*, **34**, 1548–1570.
- , M. Visbeck, R. Zantopp, and N. Nunes 2010: Interannual to decadal variability of outflow from the Labrador Sea. *Geophys. Res. Lett.*, **37**, L24610, doi:10.1029/2010GL045321.
- Gregory, D. N., 2004: Climate: A database of temperature and salinity observations for the northwest Atlantic. Canadian Science Advisory Secretariat Research Document 2004/75, 10 pp.
- Han, G., K. Ohashi, N. Chen, P. G. Myers, N. Nunes, and J. Fischer, 2010: Decline and partial rebound of the Labrador Current 1993–2004: Monitoring ocean currents from altimetric and conductivity-temperature-depth data. *J. Geophys. Res.*, **115**, C12012, doi:10.1029/2009JC006091.
- Hansen, B., W. Turrell, and S. Osterhus, 2001: Decreasing overflow from the Nordic Seas into the Atlantic Ocean through the Faroe Bank channel since 1950. *Nature*, **411**, 927–930.
- Hirschi, J., and J. Marotzke, 2007: Reconstructing the meridional overturning circulation from boundary densities and the zonal wind stress. *J. Phys. Oceanogr.*, **37**, 743–763.
- Holliday, N., S. Bacon, J. Allen, and E. McDonagh, 2009: Circulation and transport in the western boundary currents at Cape Farewell, Greenland. *J. Phys. Oceanogr.*, **39**, 1854–1870.
- Kanzow, T., and Coauthors, 2010: Seasonal variability of the Atlantic meridional overturning circulation at 26.5°N. *J. Climate*, **23**, 5678–5698.
- Kieke, D., and M. Rhein, 2006: Variability of the overflow water transport in the western subpolar North Atlantic, 1950–97. *J. Phys. Oceanogr.*, **36**, 435–456.
- Kulan, N., and P. G. Myers, 2009: Comparing two climatologies of the Labrador Sea: Geopotential and isopycnal. *Atmos.—Ocean*, **47**, 19–39, doi:10.3137/OC281.2009.
- Lazier, J., R. Hendry, A. Clarke, I. Yashayaev, and P. Rhines, 2002: Convection and restratification in the Labrador Sea, 1990–2000. *Deep-Sea Res.*, **49**, 1819–1835.
- Macrander, A., R. Kase, U. Send, H. Valdimarsson, and S. Jonsson, 2007: Spatial and temporal structure of the Denmark Strait Overflow revealed by acoustic observations. *Ocean Dyn.*, **57**, 75–89.
- Myers, P. G., 2002: SPOM: A regional model of the sub-polar North Atlantic. *Atmos.—Ocean*, **40**, 445–463.
- , and C. Donnelly, 2008: Water mass transformation and formation in the Labrador Sea. *J. Climate*, **21**, 1622–1638.
- , —, and M. H. Ribergaard, 2009: Structure and variability of the West Greenland Current in summer derived from 6 repeat standard sections. *Prog. Oceanogr.*, **80**, 93–112, doi:10.1016/j.pocean.2008.12.003.
- Osterhus, S., W. Turrell, B. Hansen, P. Lundberg, and E. Buch, 2001: Observed transport estimates between the North Atlantic and the Arctic Mediterranean in the Iceland-Scotland region. *Polar Res.*, **20**, 169–175.
- Rooth, C., 1982: Hydrology and ocean circulation. *Prog. Oceanogr.*, **11**, 131–149.
- Sarafanov, A., A. Falina, H. Mercier, P. Lherminier, and A. Sokov 2009: Recent changes in the Greenland-Scotland overflow-derived water transport from hydrographic observations in the southern Irminger Sea. *Geophys. Res. Lett.*, **36**, L13606, doi:10.1029/2009GL038385.
- Solomon, S., D. Qin, M. Manning, M. Marquis, K. Averyt, M. M. B. Tignor, H. L. Miller Jr., and Z. Chen, Eds., 2007: *Climate Change 2007: The Physical Science Basis*. Cambridge University Press, 996 pp.
- Spence, J. P., M. Eby, and A. J. Weaver, 2008: The sensitivity of the Atlantic meridional overturning circulation to freshwater forcing at eddy-permitting resolutions. *J. Climate*, **21**, 2697–2710.
- Thompson, K. R., D. G. Wright, Y. Lu, and E. Demirov, 2006: A simple method for reducing seasonal bias and drift in eddy resolving ocean models. *Ocean Modell.*, **14**, 122–138.
- Wu, P., R. Wood, P. Stott, and G. S. Jones, 2007: Deep North Atlantic freshening simulated in a coupled model. *Prog. Oceanogr.*, **73**, 370–383.
- Yashayaev, I., and J. W. Loder, 2009: Enhanced production of Labrador Sea Water in 2008. *Geophys. Res. Lett.*, **36**, L01606, doi:10.1029/2008GL036162.
- , M. Bersch, and H. M. van Aken 2007: Spreading of the Labrador Sea Water to the Irminger and Iceland basins. *Geophys. Res. Lett.*, **34**, L10602, doi:10.1029/2006GL028999.